Nonlinear dynamic response of piezolaminated smart beams

A. Mukherjee *, A. Saha Chaudhuri

Department of Civil Engineering, Indian Institute of Technology Bombay, Mumbai 400076, India

Abstract

The present paper demonstrates the effect of large deformations on the piezoelectric materials and structures under time varying loads. The energy based electromechanical piezoelectric constitutive law derived by Tiersten is adopted. For large deformation analysis of beams, a counterpart of Von Karman's plate equation is considered. The displacement fields in finite element method are based on the first order shear deformation theory. To analyze the nonlinear equilibrium equations an incremental iterative technique is employed. The control of the structure is demonstrated through a constant gain multiplier of the sensed voltage. Active control of a cantilever PVDF bimorph beam considering the nonlinear effects has been investigated.

1. Introduction

The concept of piezoelectric smart materials and structural systems with highly integrated sensors and actuators has led to a revolution in control of complex flexible structures. For high strength and highly flexible structures geometric nonlinear effects due to large deformations cannot be ignored. To control such a structure an accurate estimation of voltage sensed by the piezoelectric sensors is necessary to provide the exact remedial actuation voltage. However, research on large deformation of piezolaminated structures is sparse.

Buckling analysis of piezolaminated structures is a subset of the nonlinear problem. The enhancement of pre-buckling behavior of composite beams with geometric imperfections using piezoelectric actuators was investigated [1]. Experimental studies were carried out on the active buckling control of some composite column strips using piezo ceramic actuators [2]. A finite element analysis for active buckling of smart composite plates has been developed by Chandrashekhara and Bhatia [3]. Oh, Han and Lee [4] studied postbuckling and vibration characteristics of a piezolaminated composite plate subject to thermo-piezoelectric loads. They also worked on the thermopiezoelastic snapping of piezolaminated plates using layerwise nonlinear finite elements [5].

There are some works on large deformation nonlinear analysis of piezolaminated structures. The control of nonlinear deflection, buckling and dynamics of a circular plate with von-Karman type geometric nonlinearity was investigated [6]. A formulation on laminated composite plates with integrated sensors and actuators including large deformations was presented by Reddy [7]. An iterative finite element procedure for the analysis of piezoelectric continua including electromechanical coupling is also solved by Gaudenzi and Bathe [8]. Icardi and Sciuva [9] presented large deflection and stress analysis of multilayered plates with induced strain actuators. Geometrically nonlinear static behavior of PVDF

bimorph has been investigated by Mukherjee and Saha Chaudhuri [10].

In this paper, we present a generalized formulation for nonlinear dynamic analysis of piezoelectric structures. In the proposed formulation the algorithm presented by Bathe, Ramm and Wilson [11] is used. The formulation is extended to include the electromechanical coupling. Large deformation problems due to transverse ramp loading in presence of axial loading have been investigated for a PVDF bimorph beam.

2. Piezoelectric constitutive relations

Based on the energy principles that include electrical as well as elastic effects, Tiersten [12] presented the simplified version of linear piezoelectric constitutive equations. These equations for the kth layer of a piezo-laminated structure are

$$\text{Direct effect:} \quad \mathbf{D}_k = \mathbf{e}_k \boldsymbol{\varepsilon}_k + \boldsymbol{\xi}_k \mathbf{E}_k \tag{1}$$

$$\text{Converse effect:} \quad \boldsymbol{\sigma}_k = \bar{\mathbf{Q}}_k \boldsymbol{\varepsilon}_k - \mathbf{e}_k^t \mathbf{E}_k \tag{2}$$

where $\mathbf{D}$ = electric displacement vector, $\mathbf{e}$ = piezoelectric stress coefficient matrix, $\boldsymbol{\xi}$ = dielectric constant matrix, $\mathbf{E}$ = electric field vector, $\boldsymbol{\varepsilon}$ = mechanical strain vector, $\boldsymbol{\sigma}$ = mechanical stress vector, $\mathbf{Q}$ = matrix of elastic constants.

As direct and converse piezoelectric effects are electromechanically coupled, the voltage induced in the sensor actuates the structure as well. The actuation force $(\mathbf{e}_{31}\mathbf{E}_3^k)$ is added to the mechanical stress vector $\boldsymbol{\sigma}_x$. Therefore, after each iteration the load vector requires modification. The modified load vector, in turn, changes the voltage sensed. An iterative process evolves where we look for the convergence of the sensed voltage and the deflection.

When the piezoelectric material is poled in thickness direction only Eq. (2) can be written as follows [13]:

$$\begin{Bmatrix} \sigma_x \\ \sigma_y \\ \tau_{yz} \\ \tau_{xz} \\ \tau_{xy} \end{Bmatrix}_k = \begin{bmatrix} Q_{11} & Q_{12} & 0 & 0 & Q_{16} \\ Q_{12} & Q_{22} & 0 & 0 & Q_{26} \\ 0 & 0 & Q_{44} & Q_{45} & 0 \\ 0 & 0 & Q_{45} & Q_{55} & 0 \\ Q_{16} & Q_{26} & 0 & 0 & Q_{66} \end{bmatrix}_k \begin{Bmatrix} \varepsilon_x \\ \varepsilon_y \\ \gamma_{yz} \\ \gamma_{xz} \\ \gamma_{xy} \end{Bmatrix}_k - \begin{bmatrix} 0 & 0 & e_{31} \\ 0 & 0 & e_{31} \\ 0 & e_{15} & 0 \\ 0 & e_{15} & 0 \\ 0 & 0 & 0 \end{bmatrix}_k \begin{Bmatrix} 0 \\ 0 \\ E_3 \end{Bmatrix}_k \tag{3}$$

For a beam in xy plane σ_y,τ_{yz} and τ_{xy} are zero. Therefore, Eq. (3) reduces to,

$$\begin{Bmatrix} \sigma_x \\ \tau_{xz} \end{Bmatrix}_k = \begin{bmatrix} \bar{Q}_{11} & 0 \\ 0 & \bar{Q}_{55} \end{bmatrix}_k \begin{Bmatrix} \varepsilon_x \\ \gamma_{xz} \end{Bmatrix}_k - \begin{bmatrix} e_{31} \\ 0 \end{bmatrix}_k E_3^k \tag{4}$$

where the relation for $\bar{Q}_{ij}$ in terms of Q_{ij} are given by

$$\bar{Q}_{11} = Q_{11} + \left(\frac{Q_{16}Q_{26} - Q_{12}Q_{66}}{Q_{22}Q_{66} - Q_{26}^2}\right) Q_{12} + \left(\frac{Q_{12}Q_{26} - Q_{22}Q_{66}}{Q_{22}Q_{66} - Q_{26}^2}\right) Q_{16} \tag{5}$$

$$\bar{Q}_{55} = Q_{55} - \frac{Q_{45}^2}{Q_{44}} \tag{6}$$

The displacement field is based on the first order shear deformation theory.

$$U = u_0 - z\theta_y; \quad W = w_0 \tag{7}$$

At a distance 'z' from the reference plane the strains at any point can be expressed as

$$\begin{Bmatrix} \varepsilon_x \\ \gamma_{xz} \end{Bmatrix} = \begin{Bmatrix} \frac{\partial U}{\partial x} \\ \frac{\partial U}{\partial z} + \frac{\partial W}{\partial x} \end{Bmatrix} = \begin{Bmatrix} \frac{\partial u_0}{\partial x} - z\frac{\partial \theta_y}{\partial x} \\ -\theta_y + \frac{\partial w_0}{\partial x} \end{Bmatrix} = \begin{Bmatrix} \frac{\partial u_0}{\partial x} - z\frac{\partial \theta_y}{\partial x} \\ \phi \end{Bmatrix} \tag{8}$$

where u_0 and w_0 are the in plane and the transverse displacements at the reference plane (i.e. mid-plane) respectively and θ_y is the rotation of transverse normal about y-axis. (Fig. 1)

3. Nonlinear dynamics

The mathematical formulation for geometrically nonlinear dynamic analysis is based on the virtual work equations for a continuum within a total Lagrange coordinate system. von-Karman's large deflection theory is adopted here. For a continuum undergoing displacements the incremental equation of equilibrium of the external and the internal forces are expressed as [11]:

$${}^t\mathbf{K}_T\boldsymbol{\delta} = {}^{t+\Delta t}\mathbf{R} - {}^t\mathbf{F} - \mathbf{M}^{t+\Delta t}\ddot{\boldsymbol{\delta}} \tag{9}$$

where, $\mathbf{K}_T$ is the tangent stiffness matrix at time t, $\mathbf{R}$ is the external load at time $t + \Delta t$, $\mathbf{F}$ is the equilibrated

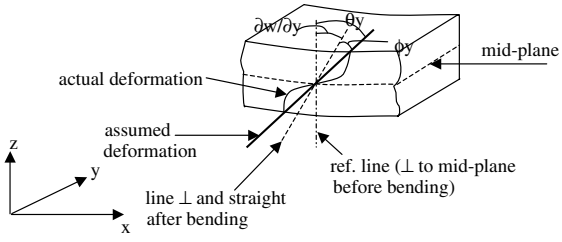

Fig. 1. Assumption of shear deformation over beam thickness.

internal force ($\mathbf{K}_S\boldsymbol{\delta} = \mathbf{F}$) at time t, $\mathbf{M}$ is the mass matrix and $\ddot{\boldsymbol{\delta}}$ is the acceleration at time $t\Delta t$.

We shall now develop the linear stiffness matrix $\mathbf{K}_0$, the secant stiffness matrix $\mathbf{K}_S$ and the tangent stiffness matrix $\mathbf{K}_T$.

3.1. Linear stiffness matrix

A three node isoparametric beam element is considered here. The quadratic variation of displacement function for bending and membrane element can be written as

$$U = \sum_{i=1}^{3} N_i u_i \quad W = \sum_{i=1}^{3} N_i w_i \quad \theta_y = \sum_{i=1}^{3} N_i \theta_{yi} \tag{10}$$

where N_i is Lagrangian quadratic shape function of the ith node of the beam.

Using Eq. 8 the strains at any point in the beam can be expressed in terms of those at the mid-plane

$$\begin{Bmatrix} \varepsilon_x \\ \gamma_{xz} \end{Bmatrix} = \begin{bmatrix} 1 & z & 0 \\ 0 & 0 & 1 \end{bmatrix} \begin{Bmatrix} \frac{\partial u_0}{\partial x} \\ -\frac{\partial \theta_y}{\partial x} \\ \phi \end{Bmatrix} = \mathbf{H}\bar{\boldsymbol{\varepsilon}}_0 \tag{11}$$

where $\mathbf{H}$ is the transformation matrix of individual lamina strain to that in the reference plane. After transforming the strains to the reference-plane of the laminated beam, we can write the element linear stiffness matrix using the principle of virtual work as follows:

$$\mathbf{K}_0 = \int_v \mathbf{B}_0^{\mathrm{T}}\mathbf{H}^{\mathrm{T}}\bar{\mathbf{Q}}\mathbf{H}\mathbf{B}_0 \,\mathrm{d}v = \int_L \mathbf{B}_0^{\mathrm{T}}\bar{\mathbf{D}}\mathbf{B}_0 \,\mathrm{d}x \tag{12}$$

where $\bar{\mathbf{D}} = b\int_h \mathbf{H}^{\mathrm{T}}\bar{\mathbf{Q}}\mathbf{H}\,\mathrm{d}z$ and b is the width of the beam.

3.2. Nonlinear stiffness matrix

The nonlinear strain displacement relationship is based on Pica et al. [14]. The additional strain produced by the large deformation effect is expressed at the following reference-plane strain vector:

$$\bar{\boldsymbol{\varepsilon}} = \begin{Bmatrix} \frac{\partial u_0}{\partial x} \\ -\frac{\partial \theta_y}{\partial x} \\ \phi \end{Bmatrix} + \begin{Bmatrix} \frac{1}{2}\left(\frac{\partial u_0}{\partial x}\right)^2 + \frac{1}{2}\left(\frac{\partial w_0}{\partial x}\right)^2 \\ 0 \\ 0 \end{Bmatrix} = \bar{\boldsymbol{\varepsilon}}_0 + \bar{\boldsymbol{\varepsilon}}_{\mathrm{L}} \tag{13}$$

where, $\bar{\boldsymbol{\varepsilon}}_0 = \mathbf{B}_0\boldsymbol{\delta}$ are linear strain components as described earlier

$$\bar{\boldsymbol{\varepsilon}}_{\mathrm{L}} = \begin{Bmatrix} \frac{1}{2}\left(\frac{\partial u_0}{\partial x}\right)^2 + \frac{1}{2}\left(\frac{\partial w_0}{\partial x}\right)^2 \\ 0 \\ 0 \end{Bmatrix} = \frac{1}{2}\begin{bmatrix} \frac{\partial u_0}{\partial x} & \frac{\partial w_0}{\partial x} \\ 0 & 0 \\ 0 & 0 \end{bmatrix} \begin{Bmatrix} \frac{\partial u_0}{\partial x} \\ \frac{\partial w_0}{\partial x} \end{Bmatrix}$$

$$= \frac{1}{2}\mathbf{A}\bar{\boldsymbol{\varepsilon}}_n$$

$$A^{\mathrm{T}} = \begin{bmatrix} \frac{\partial u_0}{\partial x} & 0 & 0 \\ \frac{\partial w_0}{\partial x} & 0 & 0 \end{bmatrix} \quad \text{and} \quad \bar{\boldsymbol{\varepsilon}} = \mathbf{G}\boldsymbol{\delta}$$

where

$$\mathbf{G} = \begin{bmatrix} \frac{\partial N_i}{\partial x} & 0 & 0 \\ 0 & \frac{\partial N_i}{\partial x} & 0 \end{bmatrix} \quad i = 1,2,3$$

The variation of generalized strain vector given by Eq. (13) with respect to $\mathrm{d}\boldsymbol{\delta}$ can be written as

$$\mathrm{d}\bar{\boldsymbol{\varepsilon}} = \mathrm{d}\bar{\boldsymbol{\varepsilon}}_0 + \mathrm{d}\bar{\boldsymbol{\varepsilon}}_{\mathrm{L}}$$

Using FE discretization it can be written as:

$$\bar{\boldsymbol{\varepsilon}} = \left(\mathbf{B}_0 + \frac{1}{2}\mathbf{B}_{\mathrm{L}}\right)\boldsymbol{\delta} \quad \mathrm{d}\bar{\boldsymbol{\varepsilon}} = (\mathbf{B}_0 + \mathbf{B}_{\mathrm{L}})\mathrm{d}\boldsymbol{\delta} = \mathbf{B}\,\mathrm{d}\boldsymbol{\delta}$$

where $\mathbf{B}_{\mathrm{L}} = \mathbf{AG}$.

3.3. Tangent stiffness matrix

In Newton–Raphson solution technique, the derivative of nonlinear equations is obtained by taking the variation of the equilibrium equations. The equilibrium equations are defined by Eq. (9), where $\mathbf{K}_T$ is the tangential stiffness matrix of the beam element and is given by,

$$\mathbf{K}_T = \mathbf{K}_0 + \mathbf{K}_{\mathrm{L}} + \mathbf{K}_\sigma \tag{14}$$

where $\mathbf{K}_0$ is the linear stiffness matrix,

$\mathbf{K}_{\mathrm{L}}$ = Large displacement stiffness matrix

$$= \int_L \mathbf{B}_0^{\mathrm{T}}\bar{\mathbf{D}}\mathbf{B}_{\mathrm{L}}\,\mathrm{d}x + \int_L \mathbf{B}_{\mathrm{L}}^{\mathrm{T}}\bar{\mathbf{D}}\mathbf{B}_0\,\mathrm{d}x + \int_L \mathbf{B}_{\mathrm{L}}^{\mathrm{T}}\bar{\mathbf{D}}\mathbf{B}_{\mathrm{L}}\,\mathrm{d}x \tag{15}$$

$\mathbf{K}_\sigma$ = Geometric stiffness matrix

$$= \int_L \mathbf{G}^{\mathrm{T}}\mathbf{S}_0\mathbf{G}\,\mathrm{d}x + \int_L \mathbf{G}^{\mathrm{T}}\mathbf{S}_{\mathrm{L}}\mathbf{G}\,\mathrm{d}x \tag{16}$$

where $\mathbf{S}_0$ and $\mathbf{S}_{\mathrm{L}}$ are linear and nonlinear axial stresses in the element.

3.4. Secant stiffness matrix

Using the stress strain relationship the equilibrium equations can be written as:

$$\int_L \mathbf{B}^{\mathrm{T}}\bar{\mathbf{D}}\bar{\boldsymbol{\varepsilon}}\,\mathrm{d}x = \mathbf{F}$$

The above equation can be rewritten as

$$\int_L (\mathbf{B}_0 + \mathbf{B}_{\mathrm{L}})^{\mathrm{T}}\bar{\mathbf{D}}\left(\mathbf{B}_0 + \frac{1}{2}\mathbf{B}_{\mathrm{L}}\right)\mathrm{d}x\boldsymbol{\delta} = \mathbf{F} \tag{17}$$

Therefore, the secant stiffness is

$$\mathbf{K}_S = \int_L \mathbf{B}_0^{\mathrm{T}}\bar{\mathbf{D}}\mathbf{B}_0\,\mathrm{d}x + \frac{1}{2}\int_L \mathbf{B}_0^{\mathrm{T}}\bar{\mathbf{D}}\mathbf{B}_{\mathrm{L}}\,\mathrm{d}x + \int_L \mathbf{B}_{\mathrm{L}}^{\mathrm{T}}\bar{\mathbf{D}}\mathbf{B}_0\,\mathrm{d}x + \frac{1}{2}\int_L \mathbf{B}_{\mathrm{L}}^{\mathrm{T}}\bar{\mathbf{D}}\mathbf{B}_{\mathrm{L}}\,\mathrm{d}x \tag{18}$$

This secant stiffness matrix is unsymmetrical. For direct iteration technique this matrix can be converted into a symmetric one [15]. Alternatively, we can find the equilibrated mechanical force vector using the equilibrium equations at every iteration. Subtracting the equilibrated force vector from the initial incremental force vector the unequilibrated force vector can be determined. The second method has been used in the present formulation.

3.5. Solution procedure

For solution of nonlinear dynamic equations several procedures are available viz. incremental procedure, stepwise procedure and iterative procedure. Among the available solution procedures, the incremental iterative method is a commonly used technique to solve large deformation problems. In the present paper, Wilson-θ step-by-step time integration scheme is employed along with incremental iterative procedure to solve the electromechanically coupled nonlinear dynamic equation. The summary of step-by-step integration is presented in Appendix A.

4. Numerical examples

To validate the developed algorithm a number of problems have been solved. This paper focuses on the large deformation dynamic effects on sensing and actuation phenomenon of PVDF bimorphs. The dimensions of the beam used in all the examples are shown in Fig. 2 and the material properties for PVDF are given in Table 1. In the present analysis damping is neglected.

As the beam is slender, the nonlinear effect is predominant in the response of the structure. The direction of the in-plane force determines the way the nonlinear analysis deviates from the linear analysis. When the in-plane force is compressive *stress softening* takes place, i.e. the effective stiffness of the structure reduces due to the presence of the in-plane stresses. As a result, the linear analysis would underpredict the deformations. A tensile in-plane force, on the other hand, *stiffens* the structure resulting in deformations smaller than those predicted by the linear analysis. In the following problems we will investigate the stress softening and the stress stiffening behavior of PVDF bimorph under transverse dynamic loading. The effect of structural nonlinearity on the generation of sensed voltage is also investigated. The active control of nonlinear vibration using a constant gain feedback algorithm is performed.

Table 1
Properties of PVDF

Elastic constant, $\mathbf{E}$ (N m^{-2})	2.0×10^{9}
Poisson's ratio, $\boldsymbol{\nu}$	0.29
Density, $\boldsymbol{\rho}$(kg m^{-3})	1800
Piezoelectric stress coefficient, $\mathbf{e_{31}}$ (C m^{-2})	0.046
Dielectricity, $\boldsymbol{\xi_{33}}$ (F m^{-1})	0.1062×10^{-9}
Maximum operating voltage (V μ m^{-1})	30

4.1. Example 1: Stress softening

In this example the nonlinear dynamic effect on PVDF bimorph is investigated. One tip ramp loading (Fig. 3) of 0.005 N is applied in transverse direction along with an axial compressive load.

The axial load varies from 0 to $0.5P_{cr}$ where P_{cr} is the 1st Euler buckling load. The nonlinear dynamic response is shown in Fig. 4. The periods of vibration increase with the increase in the axial force. The periods of vibration are 0.058 s, 0.067 s and 0.08 s for the axial loads $0.0P_{cr}$, $0.25P_{cr}$ and $0.50P_{cr}$ respectively. The effect of stress softening is evident in this example. The amplitude of vibration also increases with the increase in the

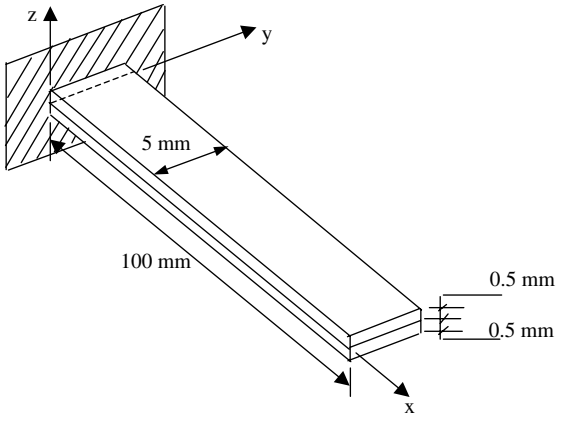

Fig. 2. PVDF bimorph.

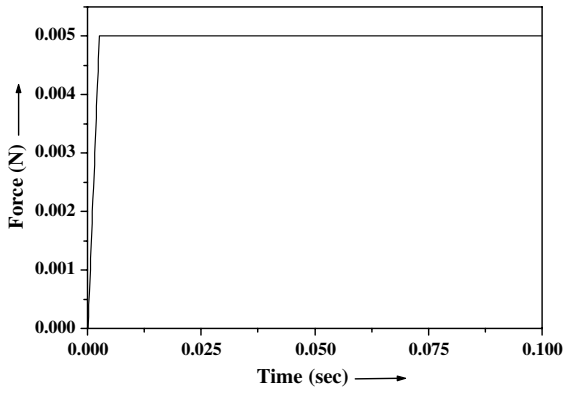

Fig. 3. Ramp load.

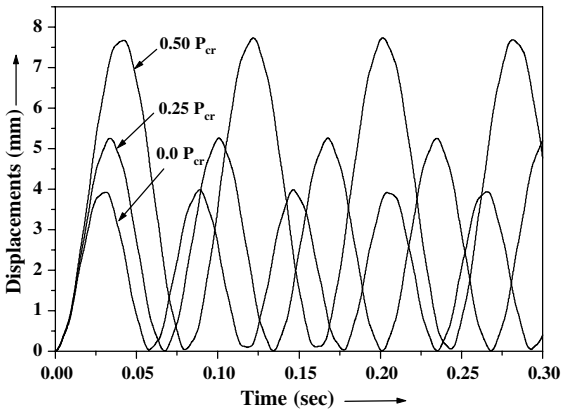

Fig. 4. Nonlinear response of PVDF bimorph due to stress softening.

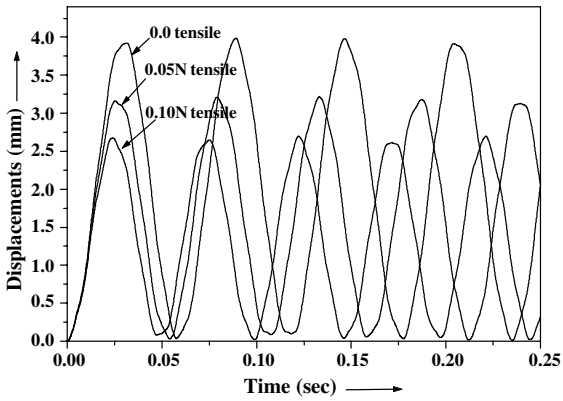

Fig. 6. Nonlinear response of PVDF bimorph due to stress stiffening.

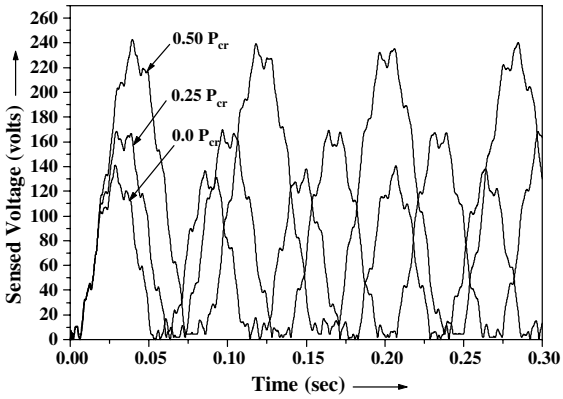

Fig. 5. Generation of sensed voltage due to nonlinear vibration of PVDF bimorph.

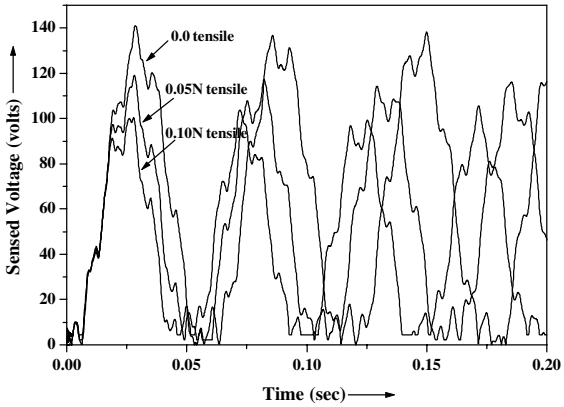

Fig. 7. Generation of sensed voltage due to nonlinear vibration of PVDF bimorph.

axial load. The peak amplitudes are 3.9 mm., 5.22 mm. and 7.66 mm. for the axial loads $0.0P_{cr}$, $0.25P_{cr}$ and $0.50P_{cr}$ respectively.

In Fig. 5 the generation of sensed voltage is shown for the response as shown above. The curves are less smooth than the displacements as the sensed voltages are proportional to the strains. The sensed voltage increases as the axial compressive force in the beam increases. The peak voltages at the root increased by 20% and 74% as the in-plane compressive force increased from zero to 25% and 50% of the Euler buckling load of the structure. Therefore, it is extremely important to include the nonlinear effects in the determination of the sensed voltage of such systems.

4.2. Example 2: Stress stiffening

In this example the stress stiffening effect of nonlinear dynamics is investigated. The same tip ramp loading of Fig. 3 is applied in transverse direction along with axial tensile load. The axial tensile load varies from 0 to 0.1 N. The nonlinear dynamic response is shown in Fig. 6. The time period and amplitude of vibration has reduced with increase in axial tensile load. The time periods are 0.058 s, 0.054 s and 0.048 s for the axial tensile force 0.0 N, 0.05 N ($0.25P_{cr}$) and 0.10 N ($0.5P_{cr}$) respectively. The corresponding peak amplitudes have reduced from 3.9 mm., 3.16 mm to 2.67 mm.

In Fig. 7 the sensed voltage is shown for the load in Fig. 3. The sensed voltage has decreased as the axial tensile force increases in the beam. The peak voltages at the root decreased to 85% and 71% for the increase in axial tensile load from zero to 0.05 N and 0.10 N respectively. It may be noted that the change in sensed voltage is more in case of compressive loads than in case of tensile loads. Hence, inclusion of nonlinear effects is more important in the presence of in-plane compressive loads than in-plane tensile loads.

4.3. Example 3: Constant gain control

In this example, vibration of cantilever PVDF bimorph is controlled with a constant gain feedback algorithm. The beam is subjected to the tip load shown in Fig. 3 and an in-plane compressive force of $0.0P_{cr}$ and $0.5P_{cr}$. In Fig. 8 the control of vibration for no in-plane loading is shown. The actuation voltage is determined by applying a constant gain (G) on the sensed voltage. The actuation load vector counteracts the mechanical load vector. Thus it attenuates the amplitude of vibration. It can be seen that for an increase in gain from 0 to 10 the period of vibration has reduced from 58 ms to 54 ms (decrease ~7%) and the peak amplitude has reduced from 3.93 mm to 3.44 mm (decrease ~12.5%). This shows the stiffening effect of the active control system.

In Fig. 9 the control of vibration in case of $0.5P_{cr}$ is shown. In this case, the increase in gain from 0 to 10 has reduced the period of vibration from 80 ms to 64.7 ms (decrease ~19%) and the peak amplitude has attenuated from 7.7 mm to 5.45 mm (decrease ~29%). It is clear that in the presence of in-plane compressive force (stress softening) the stiffening effect due to actuation is more than in the absence of in-plane compressive force. The compressive forces reduce the effective stiffness of the structure, resulting in higher deflection due to the same transverse load. As a result, the strain in the structure increases and higher voltage is sensed. This results in higher enhancement of the effective stiffness of the structure.

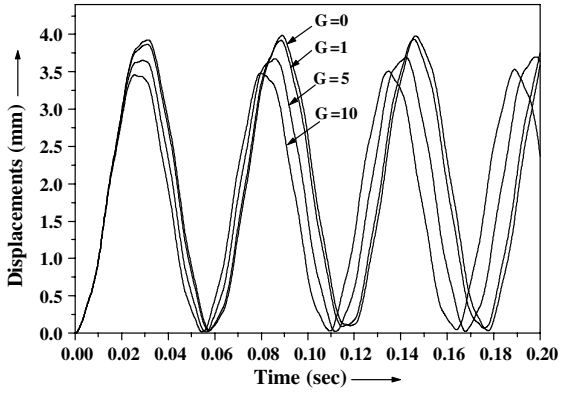

Fig. 8. Active vibration control of PVDF bimorph in linear analysis.

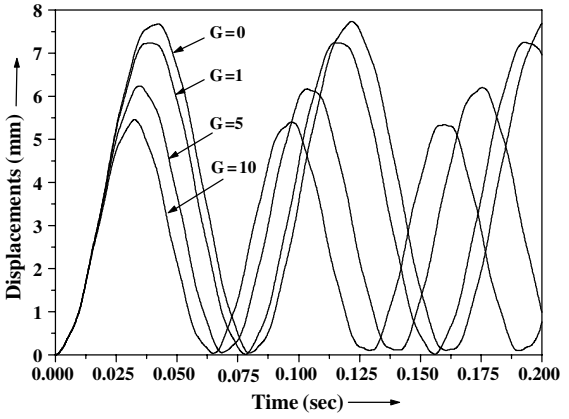

Fig. 9. Active control of vibration of PVDF bimorph in nonlinear analysis.

5. Conclusion

The geometric nonlinear dynamic analysis and control of piezolaminated beams have been presented in this paper. The nonlinear effects greatly alter the response of piezoelectric materials. In stress softening case the sensed voltage is higher than that obtained from the linear analysis. In case of stress stiffening, on the other hand, the sensed voltage is smaller than that obtained from the linear analysis. Therefore, to administer an exact remedial actuation to control such structures one must consider the nonlinear effects on the sensed voltages and actuate the structure with remedial voltages that are calculated including the nonlinear effects. In case of constant gain feedback control the effect of stiffening of the structure due to actuation increases rapidly with the increase in the in-plane compressive force. The paper considers linear piezoelectric effects only. At high strains the piezoelectric material may exhibit nonlinearities. Results including this effect will be published in future.

Appendix A. Summary of step-by-step integration

Initial Calculations

1. Form mass matrix $\mathbf{M}$; initialize ${}^0\boldsymbol{\delta}, {}^0\dot{\boldsymbol{\delta}}, {}^0\ddot{\boldsymbol{\delta}}$.
2. Calculate the following constants: tol $\leqslant 0.001$, $\theta \geqslant 1.37$, usually $\theta = 1.4$, $\tau = \theta\Delta t$ where Δt is the time increment.

$$a_0 = 6/\tau^2 \quad a_1 = 6/\tau \quad a_2 = 2 \quad a_3 = a_0/\theta$$

$$a_4 = -a_1/\theta \quad a_5 = 1 - 3/\theta \quad a_6 = \Delta t/2 \quad a_7 = \Delta t^2/6$$

3. Calculate mass contribution to effective stiffness matrix $K' = a_0\mathbf{M}$.

For each time step:

1. Calculation of displacement increment
   (i) A new stiffness matrix is to be formed using tangent stiffness matrix-

$${}^t\bar{\mathbf{K}} = {}^t\mathbf{K}_T + \mathbf{K}'$$

(ii) Form effective load vector-

$$^{t+\tau}\bar{\mathbf{R}} = {}^{t}\mathbf{R} + \theta\left({}^{t+\Delta t}\mathbf{R} - {}^{t}\mathbf{R}\right) + \mathbf{M}\left(a_1{}^{t}\dot{\delta} + a_2{}^{t}\ddot{\boldsymbol{\delta}}\right) - {}^{t}\mathbf{F} - {}^{t}\mathbf{F}_E$$

where, ${}^{t}\mathrm{F}_E$ is the electrical load vector due to actuation using a gain on sensed voltage.

(iii) Solve for displacement increments

$${}^{t}\bar{\mathbf{K}}\boldsymbol{\delta} = {}^{t+\tau}\bar{\mathbf{R}}$$

(iv) If required, iterate for dynamic equilibrium; then initialize $\boldsymbol{\delta}^0 = \boldsymbol{\delta}, i = 0$

(a) $i = i + 1$

(b) Calculate (i-1)st approximation to accelerations and displacements:

$$^{t+\tau}\ddot{\boldsymbol{\delta}}^{(i-1)} = a_0\boldsymbol{\delta}^{(i-1)} - a_1^{t}\dot{\boldsymbol{\delta}} - a_2{}^{t}\ddot{\boldsymbol{\delta}} \quad {}^{t+\tau}\boldsymbol{\delta}^{(i-1)} = {}^{t}\boldsymbol{\delta} + \boldsymbol{\delta}^{(i-1)}$$

(c) Calculate ($i-1$)th effective out-of-balance loads:

$$^{t+\tau}\bar{\mathbf{R}}^{(i-1)} = {}^{t}\mathbf{R} + \theta\left({}^{t+\Delta t}\mathbf{R} - {}^{t}\mathbf{R}\right) - \mathbf{M}{}^{t+\tau}\ddot{\boldsymbol{\delta}}^{(i-1)} - {}^{t+\tau}\mathbf{F}^{(i-1)} - {}^{t+\tau}\mathbf{F}_E^{(i-1)}$$

(d) Solve for the ith correction to displacement increments:

$${}^{t}\bar{\mathbf{K}}\Delta\boldsymbol{\delta} = {}^{t+\tau}\bar{\mathbf{R}}^{(i-1)}$$

(e) Calculate new displacement increments:

$$\boldsymbol{\delta}^{(i)} = \boldsymbol{\delta}^{(i-1)} + \Delta\boldsymbol{\delta}^{(i)}$$

(f) Iteration convergence if $\|\Delta\ \boldsymbol{\delta}^{(i)}\|_2/\|\boldsymbol{\delta}^{(i)} + {}^{t}\boldsymbol{\delta}\|_2 < \mathrm{tol}$

If convergence: $\boldsymbol{\delta} = \boldsymbol{\delta}^{(i)}$ and go to 2

If no convergence: go to (a); otherwise restart using new stiffness and/or a smaller time step size.

2. Calculate new accelerations, velocities and displacements:

$$^{t+\Delta t}\ddot{\boldsymbol{\delta}} = a_3\boldsymbol{\delta} + a_4{}^{t}\dot{\boldsymbol{\delta}} + a_5{}^{t}\ddot{\boldsymbol{\delta}}$$

$$^{t+\Delta t}\dot{\boldsymbol{\delta}} = {}^{t}\dot{\boldsymbol{\delta}} + a_6\left({}^{t+\Delta t}\ddot{\boldsymbol{\delta}} + {}^{t}\ddot{\boldsymbol{\delta}}\right)$$

$$^{t+\Delta t}\boldsymbol{\delta} = {}^{t}\boldsymbol{\delta} + \Delta t{}^{t}\dot{\delta} + a_7\left({}^{t+\Delta t}\ddot{\boldsymbol{\delta}} + 2{}^{t}\ddot{\boldsymbol{\delta}}\right)$$

References

[1] Faria ARDe, Almedia FMDe. Enhancement of pre-buckling behavior of composite beams with geometric imperfections using piezoelectric actuators. Composites Part B 1999;30:43–50.

[2] Thompson SP, Loughlan J. The active buckling control of some composite column strips using piezoceramic actuators. Compos Struct 1995;32:59–67.

[3] Chandrashekhara K, Bhatia K. Active buckling control of smart composite plates—finite element analysis. Smart Mater Struct 1993;2:31–9.

[4] Oh IK, Han JH, Lee I. Postbuckling and vibration characteristics of piezolaminated composite plate subject to thermo-piezoelectric loads. J Sound Vibration 2000; 233(1):19–40.

[5] Oh IK, Han JH, Lee I. Thermopiezoelastic snapping of piezolaminated plates using layerwise nonlinear finite elements. AIAA J 2001;39(6):1188–98.

[6] Tzou HS, Zhou YH. Nonlinear piezothermoelasticity and multi-field actuations, Part 2: control of nonlinear deflection, buckling and dynamics. ASME J Vibration Acoustics 1997;119:382–9.

[7] Reddy JN. On laminated composite plates with integrated sensors and actuators. Eng Struct 1999;21:568–593.

[8] Gaudenzi P, Bathe KJ. An iterative finite element procedure for the analysis of piezoelectric continua. J Intell Mater Syst Struct 1995;6:266–73.

[9] Icardi U, Sciuva MDi. Large-deflection and stress analysis of multilayered plates with induced-strain actuators. Smart Mater Struct 1996;5:140–64.

[10] Mukherjee A, Saha Chaudhuri A. Piezolamiated beams with large deformations. Int J Solids Struct 2002;39(17): 4567–82.

[11] Bathe KJ, Ramm E, Wilson E. Finite element formulations for large deformation dynamic analysis. Int J Numer Methods Eng 1975;9:353–86.

[12] Tiersten HF. Linear piezoelectric plate vibrations. New York: Plenum; 1969.

[13] Eisenberger M, Abramovich H. Shape control of non-symmetric piezolaminated composite beams. Compos Struct 1997;38(1–4):565–71.

[14] Pica A, Wood RD, Hinton E. Finite element analysis of geometrically nonlinear plate behaviour using a mindlin formulation. Comput Struct 1980;11:203–15.

[15] Wood RD, Schrefler B. Geometrically nonlinear analysis—a correlation of finite element notations. Int J Numer Methods Eng 1978;12:635–42.